BICAMERAL MESH ANISOTROPY

Nilanjan Mukherjee[1], Jonathan Makem[2] and Jean Cabello[1]

Meshing & Abstraction, Digital Factory, Simulation and Test Solutions, Siemens PLM Software, SIEMENS

[1] 2000 Eastman Dr., Milford, Ohio 45150 USA mukherjee.nilanjan@siemens.com, jean.cabello@siemens.com
[2] Francis House,112 Hills Road, Cambridge, UK. CB2 1PH jonathan.makem@siemens.com

ABSTRACT

This paper discusses a new approach to controlling 2D local sizing in a bicameral anisotropic mesh. We define bicameral anisotropy as a mesh size variation of two distinctly different types in two separate chambers or subdomains. The first chamber is controlled by constant to linear local size functions. The second subdomain is governed by a nonlinear sizing function leading to transitioning meshes. A controlled advancing front approach is proposed for both triangular and quadrangular meshes with the singular goal of ensuring a high local quality metric in the first chamber. An H-shock sizing scheme governs the second chamber. Virtual mesh topology is constructed at the face boundary both at geometry and nodeloop levels to facilitate this type of bicameral meshing. Results clearly indicate the efficacy of the proposed approach leading to both a well controlled desired size field and high local element quality.

Keywords: bicameral anisotropy, soft-point, virtual-vertex, sub-edge, advancing front, loop-segment, paving

1. MOTIVATION

In a large number of industrial finite element analyses problems ranging from the toy industry to aerospace, structural designers and analysts have a need to focus on specific hotspots on the surface of engineering products and their components. Typically these hotspots represent local zones of high stress, impact loading, crack growth, areas of high double curvature or areas where the field parameters studied are overly sensitive. In the automotive industry, for example, these areas could represent fillet bends in engine blocks, valve seats, seam and spot weld locations on certain areas of the car-body. In the electronic industry, these hotspots are usually more abundant and can typically represent small areas of shock and impact in drop-test simulation (cell phones for example). In the aerospace industry from leading-edge blade modeling to many nooks and corners of engine components to tire modeling, there is a strong need to zoom in on the multi-physics of local areas.

Accordingly, the finite element model for these applications demand mesh anisotropy. Usually, the mesh anisotropy desired is bicameral in more than one way. At one level bicameral anisotropy can be defined as: a) size variation within the same mesh where some elements are very small while others may be ten to a hundred times larger and b) where an average element has a large size variation (some edges of the element are small while other edges are large). Typically, most examples of anisotropy in a 2D/3D mesh bear evidence of both types of size variation. The need for anisotropy often becomes bicameral in another different way. This type of size variation is zonal, where size in one subdomain of a face is either constant or linearly varied while in the second domain size varies/transitions according to non-linear functions.

2. INTRODUCTION

Mesh gradation or anisotropic mesh size control is a relatively new research problem. The first major investigations started appearing in open literature only in the late 1990s. A couple of the early investigations focused on mesh size variation during adaptive finite element analysis [1][2], where an initial isotropic mesh is used to perform an initial solve. Next, from the error estimates computed from

the results [3][4] a size specification field is deduced (e.g. at the vicinity of each mesh vertex, the desired mesh size is specified) and the initial mesh is refined based on this field and re-solved. This process is iteratively repeated until solution convergence is achieved [5]. For surface meshes the geometric deviation or fidelity error is also computed apart from the solution error estimate which is a measure of the gap between the facets of the abstracted surface and the CAD surface. The problem faced is thus about the ways to control the mesh size variation or gradation. Borouchaki et al [6] proposed a two-way procedure to solve this problem of mesh size variation as a field problem.

Loseille *et al* [7] used an approximated Hessian-based metric field for anisotropic mesh adaption. The metric field approximates the interpolation error of the solution and is used to determine the local mesh density as well as the local element rotation and stretching. This was combined with an a-priori goal oriented error estimate for applications in the meshing of shock-dominated flows governed by Euler equations. The main disadvantage of this technique is that it cannot be applied to localized sub-division algorithms and therefore is of little practical use for problems of industrial complexity. Lecht *et al* [8] generalized a method for anisotropy detection based on the hessian of the Mach number to drive output-based adaptation for the compressible Navier-Stokes equations by using the derivative of the Mach number to guide anisotropy of the mesh. However, although the meshes are anisotropic, the value of the Mach number which governs the anisotropy is random.

Most mesh sizing algorithms reported in open literature refine meshes according to a size field computed from solution error estimates and the deviation of the mesh from CAD geometry. No particular zone of local refinement can be defined by the user and the areas of refinement do not reflect structured, layered, user-controlled meshes of high quality, especially with quadrilateral elements. The present paper proposes a novel method to address this problem.

3. BICAMERAL MESHING

To facilitate the localized zonal meshing of a region within the bounds of a larger global mesh exhibiting a different element size pattern/function, we enact the concept of *Bicameralism*, whereby a local and a residual global chamber (C_1 and C_2 respectively) are meshed with different element size pattern/functions (S_1 and S_2 respectively), as shown in figure 1. The parent face, F, may be defined as the boolean union of the local and residual chambers given by

$$F = C_1 \cup C_2 \tag{1}$$

Similarly, the final mesh, M on the parent face can be defined as the boolean union of the meshes in the local and residual chambers (M_1 and M_2 respectively) expressed by

$$M = M_1 \cup M_2 \tag{2}$$

For tri meshing the bounds of the local chamber is circular and square for quad meshing, as shown in figure 1.

4. PROPOSED ALGORITHM

The problem to be addressed is defined by the following user specified input data data –

i) surface geometry (tessellated)

ii) a global size s_g with which the entire surface is supposed to target

iii) *mesh points* or points on the surface, on edges and/or vertices that have a local size definition different from s_g.

iv) a radius or square of influence (**R**) at each point in (iii) which denote the chamber of influence and

v) (optionally) a size variation function $g(r)$ for each chamber. If the function is not specified by the user, the mesher assumes constant size.

The problem at hand, is thus clearly bicameral, i.e. it is split into two separate chambers with clearly defined boundaries. Chamber I is called *local chamber* and is defined by the radius or square of influence specified by the user around certain points which are the origins of the local size field. The source or origin of a local chamber can be of three types of mesh points -

a) face interior mesh point

b) face vertex

c) edge-interior mesh point

Chamber II represents the rest of the geometry to be meshed and is called *global-residual chamber*. In the global-residual chamber the mesh size first transitions from the local size to global and then stabilizes to a field normal value which is the global size of mesh generation.

5. VIRTUAL GEOMETRY CREATION FOR LOCAL SIZE CONTROL

In order to bound the local mesh size chamber modifications to the physical domain of the problem, i.e., the boundary of the local chamber, need to be made. This is done by creating virtual geometry both on the boundary and interior of the face around the origin or source of the local chamber.

5.1 Creation of 0D and 1D Virtual Geometry

0D and 1D virtual geometry are created using both finite element nodes and the parent geometry to efficiently expedite mesh sizing around mesh points with local size. This is done using *soft-points, virtual-vertices, sub-edges* and *loop-segments*.

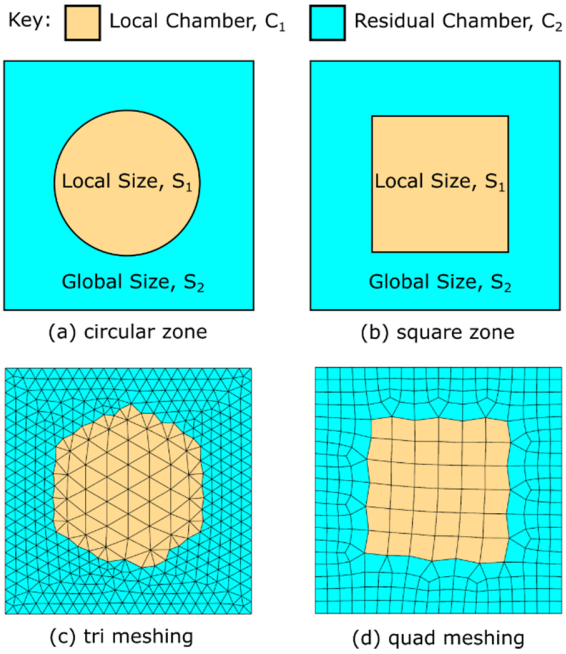

Figure 1 Bicameral Mesh Sizing

5.11 Creation of Local "Soft-Point" limiters

If local size is defined at a vertex or on a mesh point created in the interior of an edge, we intersect the circle (of the radius of influence **R**) with all edges meeting at the mesh point or vertex as shown in Figure 2. A node is created at the points of intersection prior to mesh generation. These nodes are called *soft-points*. They are "soft" in the sense they are not required to be created at these locations by the application. Instead, meshing algorithms create these nodes for the purpose of pre-seeding edges at specific locations, in this case as mesher-native vertices called *virtual-vertices*. A virtual-vertex is nothing but a soft-point which is a special type of node. The special property that distinguishes it from other nodes is that they are semi-permanent – they are not deleted if the mesh is deleted on the faces that share the edge, they remain similar to vertices. A virtual vertex can only be selectively deleted by a meshing function.

5.12 Creation of Sub-Edges

Figure 3 describes the next step, where the edge is virtually partitioned into segments called virtual *sub-edges*. In terms of node-geometry and face-edge association the edge owning the mesh point is still unique and undivided. For the purpose of mesh generation, however, it is sectioned into virtual sub-edges where each sub-edge is meshed as a separate entity.

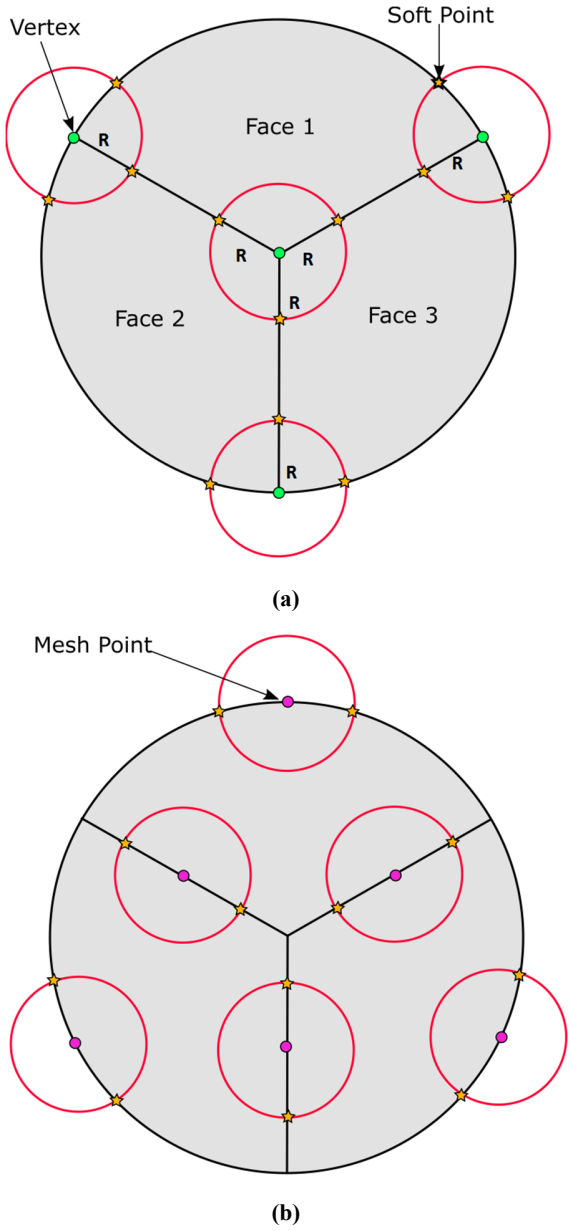

Figure 2. Local size on mesh point on edge (a) at the vertex, (b) in the interior.

This allows us to create different size distributions on the sub-edges. The sub-edge is a child of the geometry edge. Sub-edges can be deleted at any time if the virtual vertices on the parent edge are deleted, but the parent geometry edge will stay intact.

Two virtual-vertices can approach each other as shown in Figure 4, if there are local size definitions at the two end vertices of an edge and the radii of influence of both are such that the circles come close or overlap. In such situations only one soft-point or virtual vertex is created at the mid-point of the overlap zone.

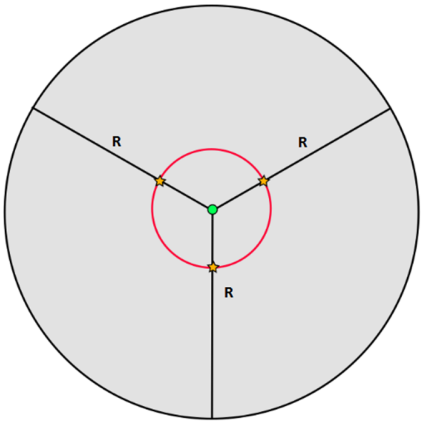

(a) soft points marking sub-edge extremeties

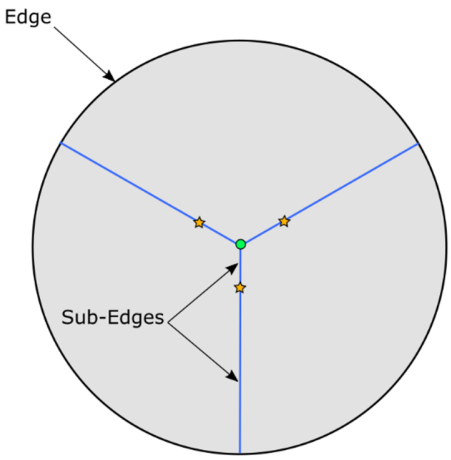

(b) sub-edge creation

Figure 3. Virtual sub-edges.

5.2 Distribution of Local Size Information

Once all mesh points with local size are processed creating 0D and 1D virtual geometry, the faces are ready for mesh generation. The boundary edges of all faces are discretized according to the size information they own. Next, the discretized face-loops, now called *node-loops* are laid down in 2D for mesh generation. At this point, the local size information existing on the mesh point/virtual vertex – the size value and the radius of influence – need to be applied to certain boundary segments of the nodeloop. These segments of the nodeloop will be called *loop-segments* from here on.

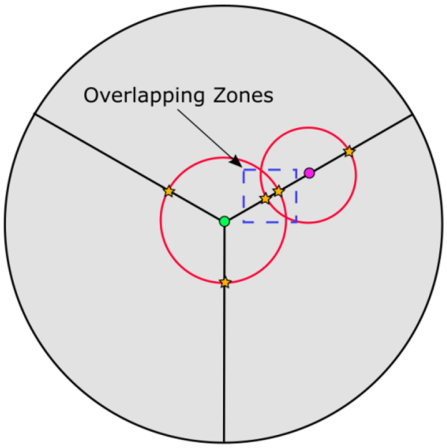

(a) zonal encroachment

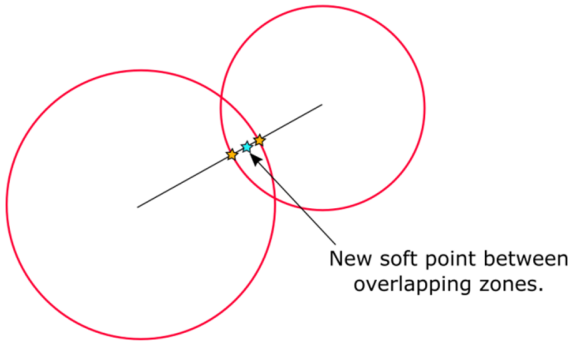

(b) soft point repositioning

Figure 4. Overlapping circles of influence

6. LOOP SEGMENT GENERATION

Once all virtual geometry is constructed, the face boundaries are completely discretized, the face is laid down or flattened into a 2D domain, node-loops defining the boundaries of the 2D area to be meshed are created. Certain segments or parts of such a node-loop are called loop-segment. A typical loop-segment is shown in Figure 5. The loop-segment $\mathbf{L_s}$ basically defines the part or segment of the face boundary that falls within the radius of influence bound by soft-point limiters $\boldsymbol{s_0}$ and $\boldsymbol{s_1}$ (Fig.5) and can be expressed as

$$\boldsymbol{L_s} = \sum_{i=s_0}^{s_1} \boldsymbol{l_{fi}} \quad \boldsymbol{in\ explicit\ domain}\ (\boldsymbol{s_0}, \boldsymbol{s_1}) \quad (3)$$

and where l_{fi} denotes the i-th loop-front as described by the CSALF [9,10] algorithms.

It is important to note that the local chamber has a shape which is decided by the user. If the user does not specify the shape of a local chamber, circles are used for triangular

elements and square shape for quadrangular. These two chamber shapes are used throughout the present paper. However, the overall algorithm is shape-independent as the chambers are filled with advancing front meshes which can cater to any general shape. For most industrial meshes analysts focus on either circular or square shaped chambers.

6.1 Partial Paving/Advancing Front on Face Boundary

Paving or Advancing Front [9,10] have been around for the past three decades and are the most popular of triangular and quadrangular surface mesh generation algorithms today. The CSALF algorithms however [11,12], are largely improvised adaptations where more control is exercised on advanced/paved layers and the front advancing strategy is amalgamated with a mesh-area subdivision technique making it a rather hybrid approach. This hybrid paving/advancing front strategy is further specialized to create best quality elements in the local chamber within the radius of influence.

6.11 Creation of Loop Segments

Since the loop-segment is part of the face boundary that falls within the radius of influence **R**, it must be discretized at the local size along with the circular arc between them. In Figure 5, the red segment on the face boundary defines the

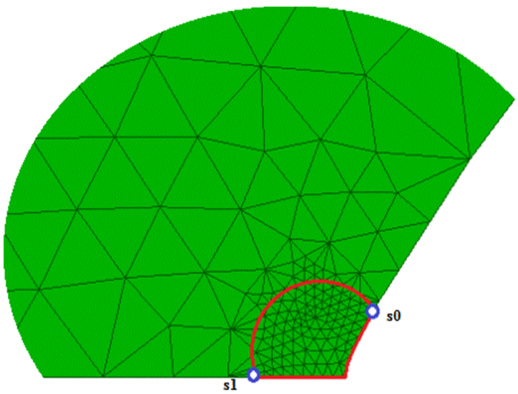

Figure 5. A typical loop-segment

loop-segment. As expected, the size of discretization along this segment reflects the local size defined at the vertex. The area inside the red circular arc defines the portion of the mesh area or nodeloop inside the radius of influence. The mesh size in this zone reflects the local size defined. The blue circles mark the soft-points or virtual vertices created on the edges incident at the corner vertices s_0 and s_1. These mark the start and end of the loop-segment and the intersection of the circle of local size influence and the edges joining the source or origin of the local chamber.

6.12 Types of Loop Segments

Three types of loop-segments are dealt with, as shown in figure 6. Two of them are edge-based and the third one is in the interior of the face. These are :

Vertex-based or edge-end loop-segment

When the local size control is defined at a vertex, the loop segment covers all edges incident at that vertex. Figure 5 shows a classical vertex-based loop segment for a circular local chamber. Any edge-based loop-segment is defined by at least three points – the virtual vertex on connected edge 1, the vertex of the edges or the origin of the local chamber where local size is defined and the virtual vertex on connected edge 2. The loop-segment starts at virtual vertex A and runs up to virtual vertex B as shown in Figure 6a.

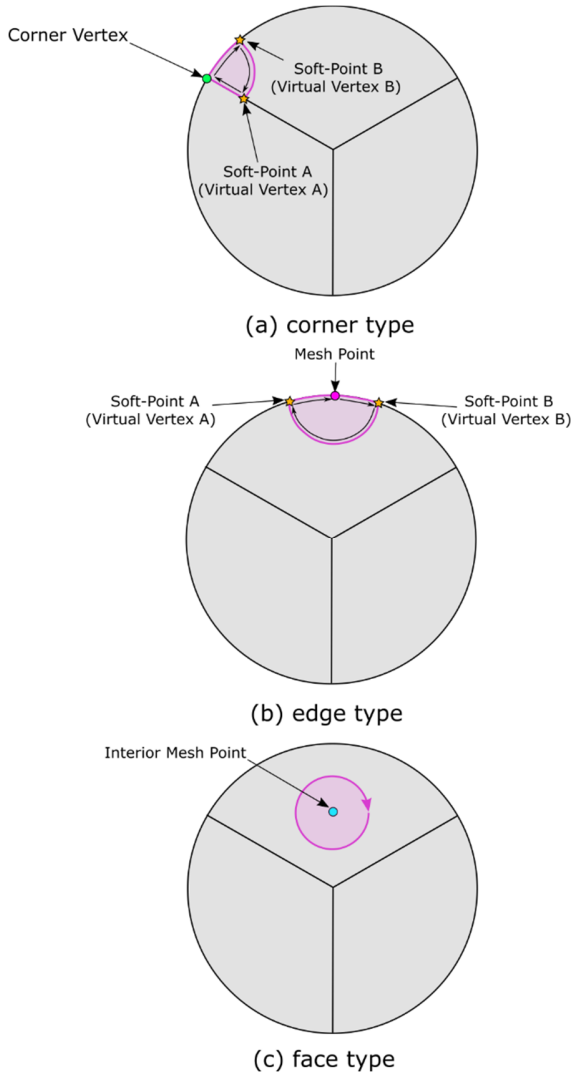

Figure 6. Loop segment types

Edge interior loop-segment

This second type of loop-segment is also defined by 3 points – starts at virtual vertex A, touches the origin of the local

chamber, the mesh point on the edge and runs up to virtual vertex B (Figure 6b).

One point loop-segment

The third type of loop-segment is a one-point loop defined by the mesh point in the interior of the face (Fig.6c).

6.13 Creation of Face-interior Point Loops

Face interior mesh points with local size control are first appended to the face topology as new one-point loop-segments. Next, we pave around the point at local size gradually expanding the area covered by elements to the circle of influence. This is described in Figure 7,9 and 10.

Once paving stops as we reach the radius of influence **R**, the free-edges of the cluster of elements form a closed node-loop as shown in Figure 10. The boundary of the white shaded area in Figure 10a and that of the orange shaded area in Fig. 10b define the new loop.

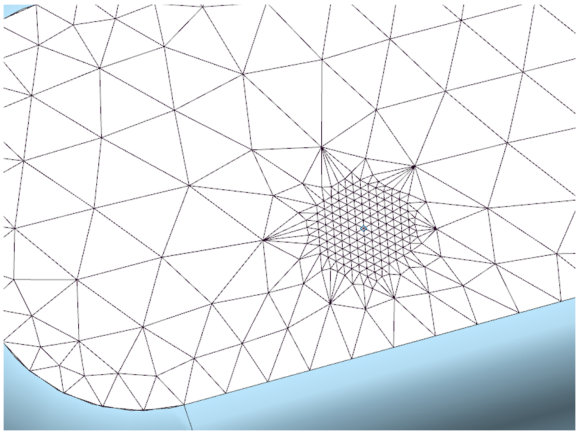

Figure 7 Face-interior point loop

This nodeloop replaces the single-point loop as part of the face topology. Therefore, in a nutshell, paving/advancing front of the single point-loop produces a new face interior loop as output which is added to the face thus altering its face topology for meshing the residual-global chamber. An example for how it is done is illustrated in Figure12.

6.14 Creation Partial Paving/Advancing Front Meshing of Edge Loop Segments

The acronym CSALF stands for Combined Subdivision and Loop-Front mesher. The mesh area of the face is defined by node-loops. Every three adjacent nodes form what is called a "loop-front". Each loop-front is advanced based on an angular advancement template and terminated based on front-type pair based closure stencils [11,12].

When all loop-fronts that form the node-loop have been advanced, a new nodeloop results. This is how the node-loops are advanced – the outer moves inwards, the inners move outward. When they collide, loop-front advancement is arrested and the remaining mesh area is filled. CSALF meshers, therefore, are "symbiotic" in the sense they alloy two distinctly different mesh generation algorithms working recursively in tandem. Figure 8 shows two examples of loop-segment paving/advancing front with quadrilaterals and triangles.

In order to advance the fronts for the loop-segments the same CSALF meshers are used with more improvisation and tighter control. For edge-based loop-segments, we resort to partial advancement of the boundary in the sense elements are first created only along the length of the loop-segment $\boldsymbol{L_s}$ defined in equation (3). When the circle or square of influence is all filled with these high quality elements, the mesher stops meshing chamber I. The free element edges of the cluster of elements created become a new node-loop which is inserted/appended to the face topology as shown in Figures 8-10 for both quadrilaterals (paving) and triangles (advancing front). The triangles created can be ideally equilateral or right-angled depending on the user's choice.

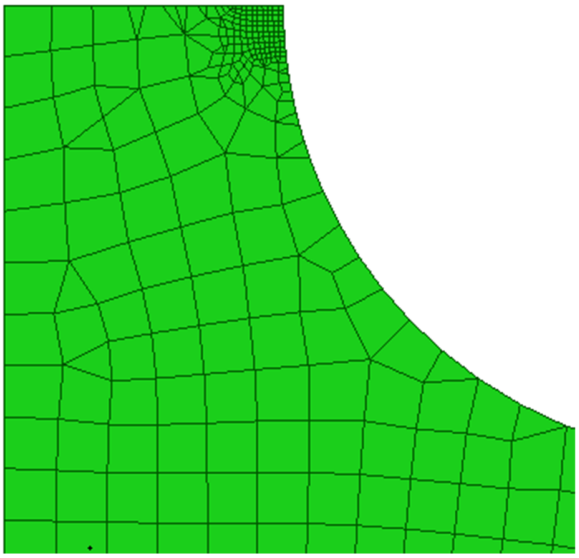

(a)

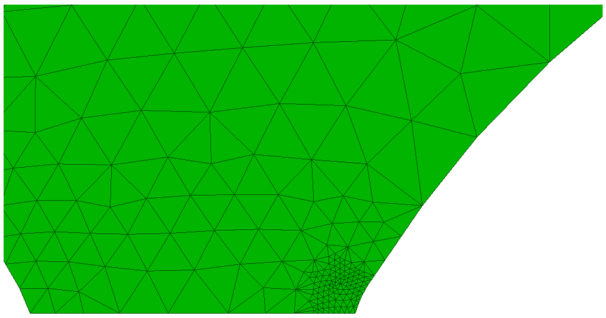

(b)

Figure 8. Partial paving (a)/ Advancing Front (b) on faces with local size on a boundary vertex.

The face-inserted loops are next joined up with other interior loops and the outer nodeloop to create a single connected nodeloop that represents the residual-global chamber II. The same CSALF mesher meshes chamber II next.

6.15 Partial Paving/Advancing Front Meshing of Face-interior Point-Loop

For face-interior single point node-loops, the approach is different. In case of Advancing Front meshing with triangles, first six equilateral triangular elements are created around the point. Advancing loop-fronts continue and more layers of equilateral triangles result around the mesh point with local size until the circle of influence is covered as shown in Figure 10a. Loop-front advancement stops and the new nodeloop formed by the free element edges of the element cluster are appended to the mesh area.

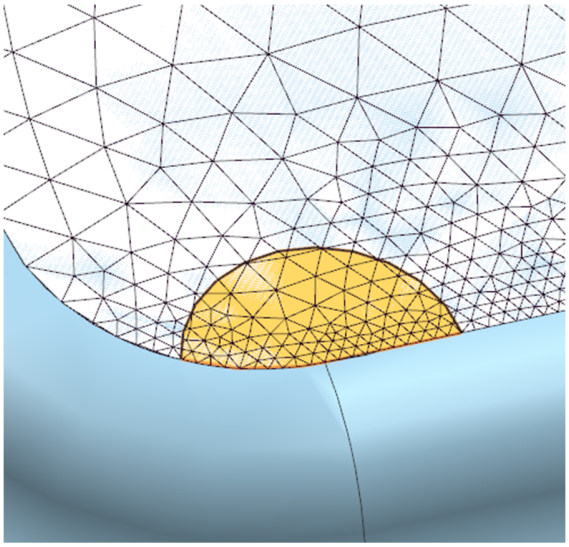

Figure 9. Paving/Advancing Front of an edge-based (vertex) loop-segment resulting in a new boundary loops.

In the case of paving with quadrilaterals, the question of direction of loop-front advancement arises, especially when the shape of the local chamber is expected to be rectangular. This is not an issue with advancing front meshing with triangles where the elements grow radially outward in all directions. Thus, for quads, if a direction vector is supplied by the user, four quadrilateral elements (2X2) created oriented along that direction. As paving continues, more layers of right-angled square elements are added until the circle of influence is entirely covered (Figure 10b). For quadrilaterals we create one or two additional layers beyond the circle of influence to allow for elegant mesh transitioning.

6.16 Local Chamber Collision

When the sources of local chambers are face-interior and the local chambers are in fair proximity, chamber collision is probable. Loop-front advancement is done one layer at time for each loop. Consequently, as loop-fronts advance from the origins of two face-interior local chambers as depicted in Figure 11, collision is detected. As soon as it happens, front advancement for the chamber in the collision zone is arrested as shown below.

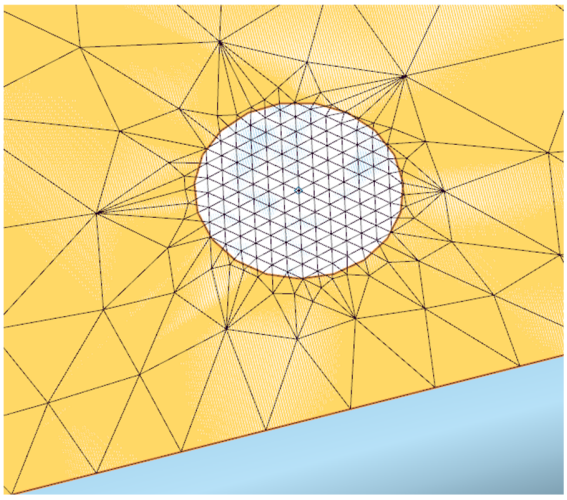

(a)

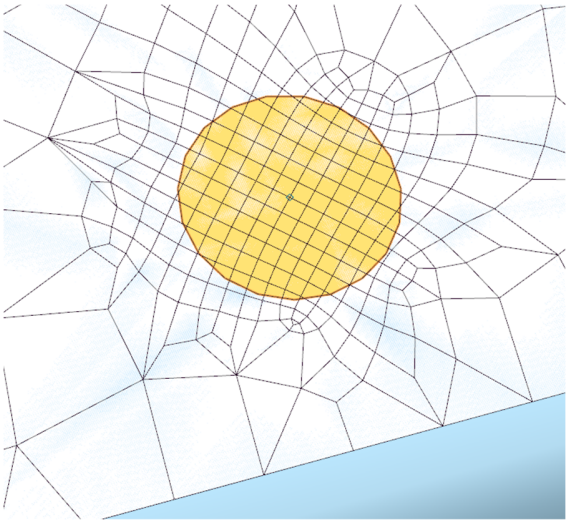

(b)

Figure 10. Partial paving (a)/ Advancing Front (b) on faces with local size on interior point.

Figure 12 depicts the nodeloop boundaries of the colliding local chambers when their growths are both arrested. These face-inserted loops are next joined with the outer nodeloop (and other inner nodeloop). Figure 13 shows the final mesh.

While paving/advancing front mesh generation in chamber I (as in case described by Figure 6a where three faces meet at one corner), the mesher first covers all local chambers (chamber I) of each face connected at the vertex. In case of the type of local chamber described in Figure 6b, the chamber is on the face-edge but not shared with other faces, whereas in Figure 6c, the local chamber is completely interior to the face.

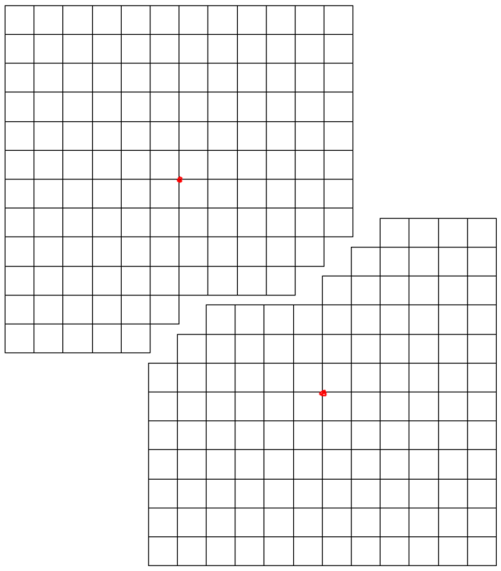

Figure 11. Chamber collision in the interior of the face.

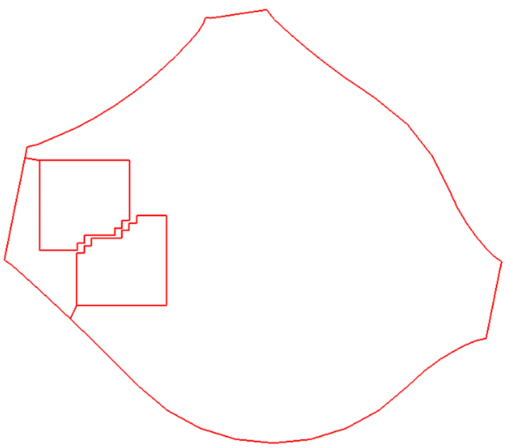

Figure 12. Truncated colliding local chambers joined with the outer face-boundary.

7. BICAMERAL SIZE CONTROL

Bicameral anisotropy can be variegated but at least binary in the limit. The size in each local ring or square of influence (local chamber) can vary according to a different local function. This paper only discusses constant to linear functions in the local chamber. Let us assume, the mesh size field in chamber I, is defined by F(I). The center or source of the chamber is point $\overline{P}$ from where the desired local size field originates. The field needs to be varied according to a user-defined function g, whose domain for a circular shape is expressed in polar coordinate system as

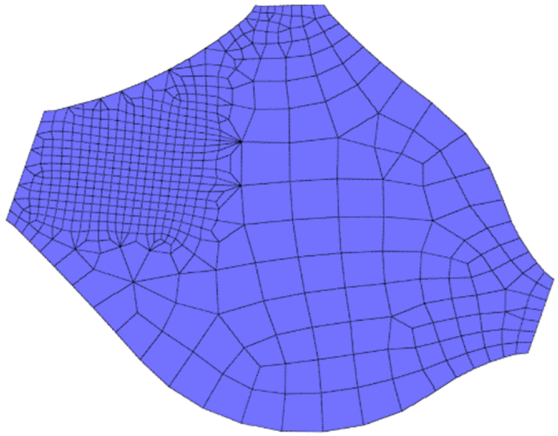

Figure 13. Final quadrilateral mesh on the face with interior local chamber origins.

$$F(I) = g(r) \quad in \ explicit \ domain \ (0, R) \qquad (4)$$

where R = Radius of influence

and redefined for a square shape in a Cartesian coordinate system as

$$F(I) = g(x) \quad in \ explicit \ domain \ (\overline{P} - R, \overline{P} + R) \quad (5)$$

Figures 9-12 provide ample examples of such variations in local size. The sizing function in the residual-global chamber (also known as chamber II) is a H-shock variation function expressed succinctly as

$$F(II) = \acute{h}_{AB} \qquad (6)$$

where $\acute{h}_{AB}$ describes a shock type sizing function which is explained later in section 7.2.

7.1 Various Aspects of Local Size Control

In contrast with previously reported mesh sizing algorithms discussed in section 2, this algorithm also provides numerous user-driven ways to vary or regulate mesh size. Size variation can be controlled on edges connected to a vertex with local size even outside the radius of influence, at least two different triangular element types can be provided as option, local mesh size control can be made coarser (Figure 14) instead of finer and finally, within the radius of influence, thickness of layers can be varied. We provide a default behavior for each one of these options based on a best practice standard.

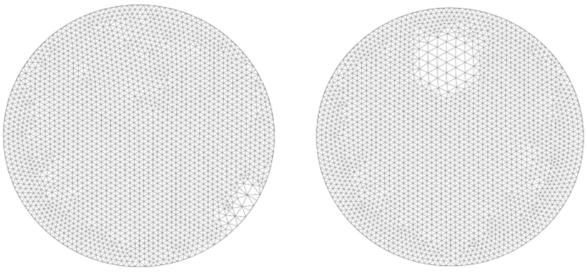

(a) (b)

Figure 14. Coarser local size on the face boundary (a) and interior (b) in a finer size mesh.

7.11 Mesh Sizing on Edges With Size Control

To ensure better mesh size transition and element quality, our algorithm varies mesh size even outside the radius of influence on edges. Figure 15 explains size distribution scheme on edges incident on a vertex with local size control. The mesh size is kept constant at its local value s_0 within the radius of influence **R**. Over the next **2R** length, on all edges connected to the vertex, the size is varied parabolically up to 50% of the global size s_g. Over the remaining length of the edge mesh size increases from $s_{/g2}$ to s_g following the H-shock size variation algorithm [6]. Equation family 7 describes the size function g (x) on the edge of length l as

$$g(x) = s_0 \quad where \quad R \geq x \geq s_0$$

$$g(x) = s_0 + bx^2 + cx \quad where \quad R + 2R \geq x > R$$

$$b = \frac{s_g - 2s_0}{12R^2} \text{ and } c = \frac{s_g - 2s_0}{12R}$$

$$g(x) = \frac{s_g}{2} f(H_s) \quad where \quad l \geq x > (R + 2R) \tag{7}$$

Figure 16 shows how controlled, multi-staged bicameral size variation avoids the local size from over-spilling too far into the edge and the connected faces. Figure 16a depicts a size transition with the H-shock method applied immediately outside the radius of influence on all edges connected to the vertex with local size. The finer size seems to over-penetrate into the edges and thus their owning faces. The effect of a multi-staged controlled size variation as described above reduces the "spill effect" as shown in Figure 16b. Beyond length = R on the meeting edges, the size is varied parabolically over 2R length and graded up to global size thereafter. Many users prefer the latter scheme while some might like a less drastic transition as in the former.

Furthermore, the size variation type in stage II (over the length of 2R) is also optional. Users could use a linear or geometric progression variation instead of the default parabolic type. A contrast of geometric progression variation versus parabolic is demonstrated in Figure 17.

7.12 Control of Triangular Element Types

Two different triangular element types can be provided as option especially for mesh generation within the radius of influence on edges. A 90-degree triangle can be used (Figure 8b) optionally although the best element perhaps is an equilateral triangle (Figure 7).

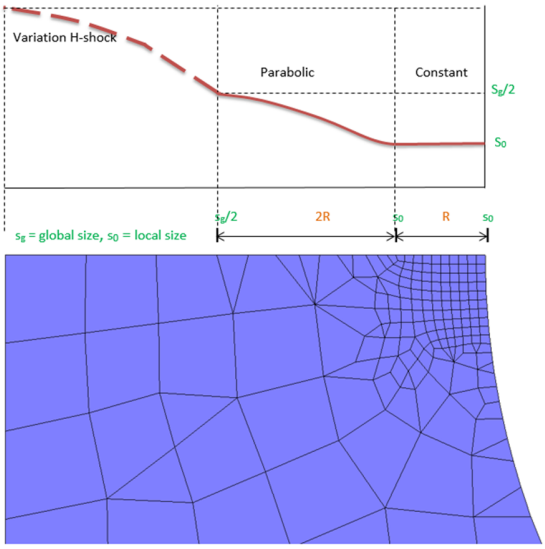

Figure 15. Mesh size distribution scheme on edges with local size on vertex.

7.13 Coarser Mesh Size Local Control

The local chamber mesh size does not necessarily have to be finer than the residual-global mesh size. Mesh size at mesh points or vertices can be made coarser instead of finer. Our approach handles such "reverse variation" systems with ease and elegance. Sizes get bigger within the radius of influence and reduce to global size outside the local zone. Figure 14b shows examples of reverse size variation.

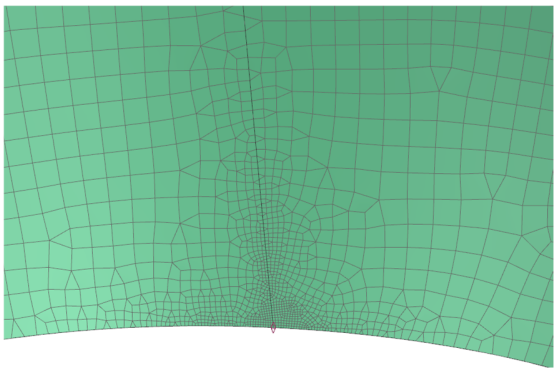

(a)

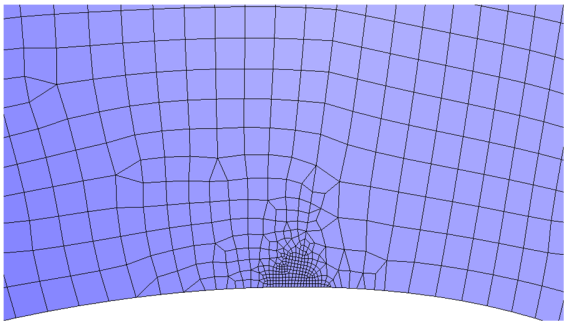

(b)

Figure 16. Size transition effect with controlled bicameral size distribution s on edges – H-shock based mesh size transition immediately beyond radius of influence (a) versus a staged constant-parabolic-H-shock variation (b)

7.14 Through-Layer Element Thickness Variation

Bicameral mesh anisotropy by definition allows both controlled and uncontrolled mesh size variation in the local and global-residual chambers. For example, within the radius of influence, thickness of mesh layers can be varied by any function specified by the user. Figure 18 depicts a quad mesh on a fan casing (b) where a local box-size variation is applied at the center of the casing that follows a Fibonacci function.

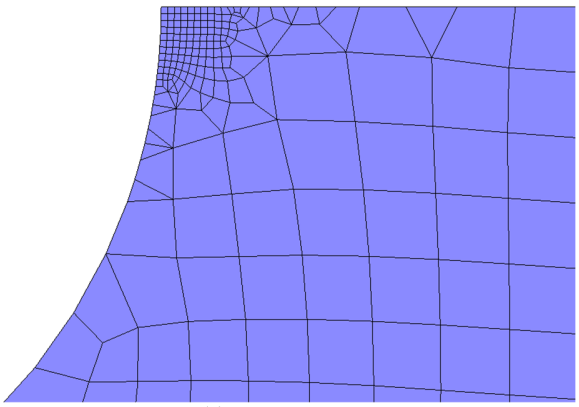

(a)

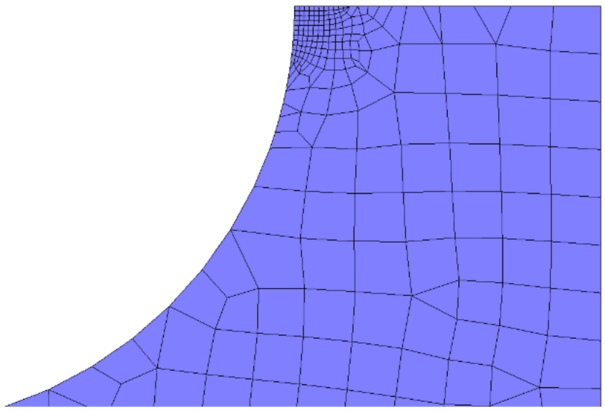

(b)

Figure 17. Size distribution schemes on edges with local size on vertex – geometric progression (a) versus parabolic (b)

A total box thickness (2L) of 20 is desired in 6 layers. The radii R_n or half-thickness of each box layer variation can be expressed by the function family

$R_n = R_{n-1} + (F_n / \sum_{n=1}^{6} F_n)L$ where the Fibonacci sequence is expressed as $\{F_n\}_{n=1}^{6}$; $R_0 = 0$ and the linear recurrence equation is

$F_n = F_{n-1} + F_{n-2}$ with $F_1 = F_2 = 1$ (8)

The 6-layered local chamber mesh around the blue point of application on the fan cover is shown in Figure 18a.

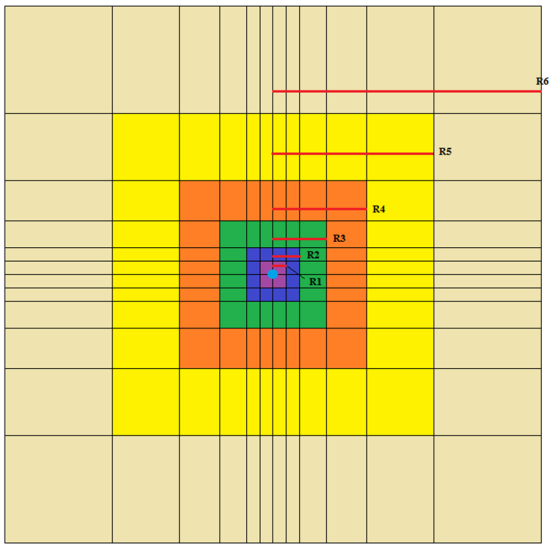

(a)

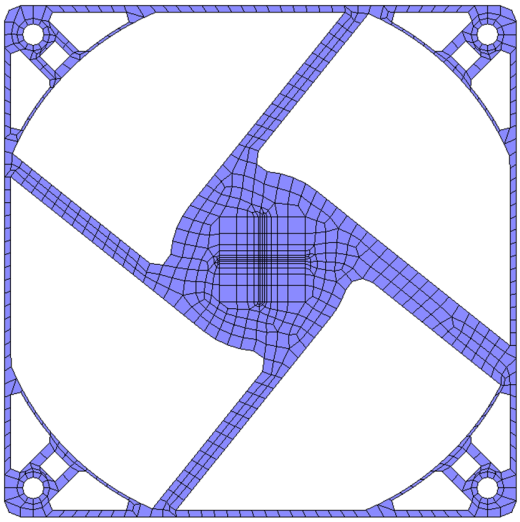

(b)

Figure 18. Six layers of Fibonacci size variation in a local chamber (a) on a fan casing (b)

7.2 Mesh Size Transition in the Global-Residual Chamber

Beyond the radius or boxes of influence of the local chambers lies the global-residual chamber, which is the rest of the surface area. In this chamber mesh size, on both edges and faces, is varied/transitioned following the previously published H-shock algorithm [6]. Borouchaki et al introduced notions of H-variation and H-shock associated with a control space and two correction procedures called H-corrections. Size variation in a control space can be defined in two different ways - gradient of a size function h, and the ratio of the Euclidean length of two adjacent edges. The H-variation measures the gradient of the function h, while H-shock represents the mesh gradation along an edge PQ and measures the distortion of interpolation function h along it. The H-correction factors tune the size variation factor at a point on the surface in all directions. An H-shock sizing function is developed based on the size-map or the background mesh used. For any edge AB of the triangular background mesh of length $\mathbf{l_{AB}}$ in Euclidian space, the H-shock size for the edge is expressed as

$$h_c(AB) = \max\left(\frac{h(B)}{h(A)}, \frac{h(A)}{h(B)}\right)^{\frac{1}{l_{AB}}} \qquad (9)$$

which represents the mesh gradation along the background element edge AB. This is a measure of the distortion of the sizing function h along the edge. This H-variation can be defined at the vertices of the background mesh by considering the measures related to the adjacent edges. An edge shock (H-correction) correction is also used. The edge shock correction tries to guarantee that the size shock is bounded by a certain user defined value β.

We set out to assume a geometric variation of the size function

$$h_t = h_A\left(\frac{h_B}{h_A}\right)^t \qquad \text{and}$$

$$l_{AB} = |AB| \int_{t=0}^{1} \frac{1}{h_t} \, .dt \qquad (10)$$

Analytically equation (10) can be recast as

$$l_{AB} = |AB| \frac{h_A - h_B}{h_B . h_A . Log\left({}^{h_B}/_{h_A}\right)} \qquad (11)$$

A dilemma arises when $h_B > h_A$ and $h_c >$ β around the decision about which one to keep. We vouch for the lower value. Under this condition, h_B is modified as

$$h_{Bnew} = \gamma h_B \text{ where } \gamma = \frac{\beta}{h_c(AB)} \qquad (12)$$

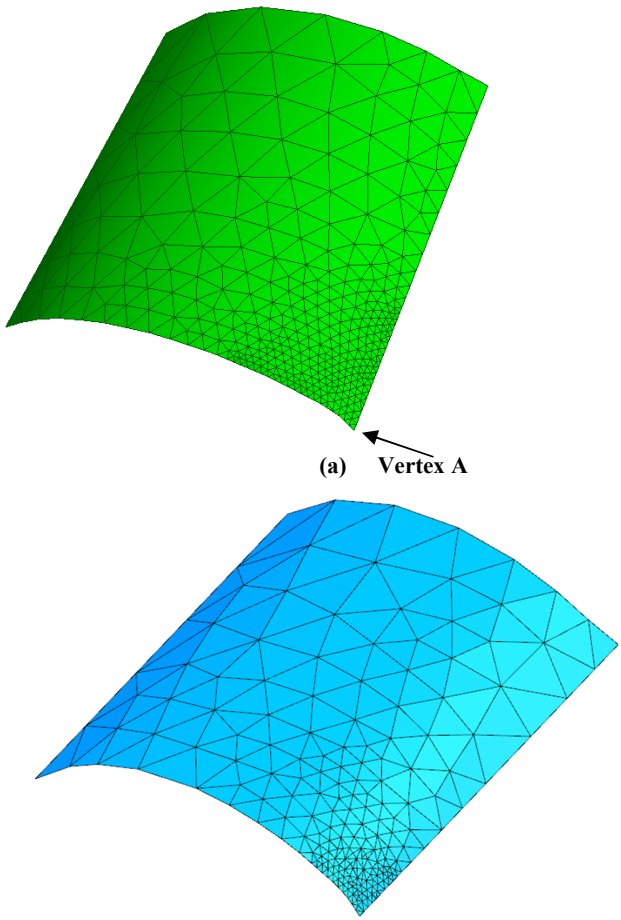

Figure 19. Comparison of size transition effect on a curved face with local size on vertex. H-shock transition (a) versus Bicameral anisotropy (b).

Figure 19 shows two images of transitioning meshes on a curved plate with local size on one vertex. The global size s_g = 8 and local size s_l at the lower right vertex A = 0.5 with a radius of influence **R** = 5.0. Figure 19a shows the H-shock variation in comparison to bicameral anisotropy in 19b. In Figure 20. we compare the size variation along the diagonal line joining opposite vertices of the face starting at vertex A. With H-shock type variation alone, the size field normalizes to global size at a much flatter gradient as is evident in the figure. In the case of bicameralism, the element size sharply grows to global size outside the zone of local influence.

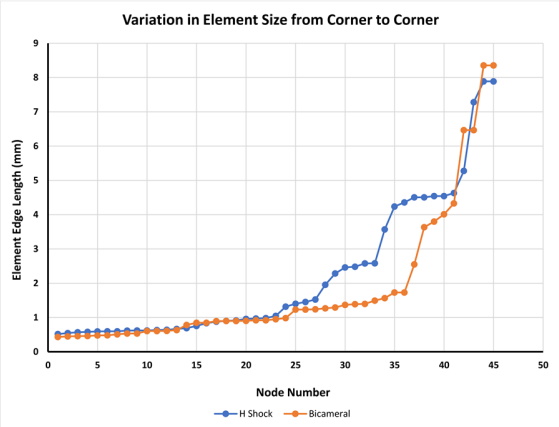

Figure 20. Comparison of variation in element size between H-Shock Variation and Bicameral Anisotropy.

7.3 Weighted Half-Edge Method (WHEM) Flattening

The present meshing algorithm is developed in 2D and is employed on the flattened 2D domain of the face. The Weighted Half-Edge Method for 2D parameterization of a tessellated 3D face has been developed at Simulation and Test Solutions, Siemens over the past decade by Beatty & Mukherjee [13]. The method developed for both linear and nonlinear problems uses a compromise between conformal mapping (preserving triangle shape) and authalic mapping (preserving area or triangle altitude) to generate 2D domains with highly reduced transformational distortion. The meshes (both local and global) are generated in this 2D domain and transformed back to 3D space.

7.4 Controlled Variational Smoothing

The final mesh produced on the entire surface is smoothed by a variational smoother [14] which applies a variety of algorithms for node movement depending on the valency of the node (i.e. the number and types of elements connected to each node). For both triangular and quadrilateral meshing we create ideal or perfect quality elements within the radii of influence. Therefore, care is taken to not disturb them too much during mesh smoothing. The variational smoother is modified by inverse length-weighing to ensure mesh size gradients are not flattened out too much. Inverse length weighing constrains the smoother within the radii of influence so as not to disturb the elements created inside those zones or sub-areas.

8. ADVANTAGES OF ADVANCING FRONT APPROACH IN BICAMERAL ANISOTROPY

There are many ways of dealing with functional control of local and global anisotropy and their interaction, where the field equations varies. The use of a novel advancing front approach in such problems of bicameral anisotropy, as described in this paper, has many advantages and unique properties. Let us try to quantify the benefits in terms of its performance, efficiency and cost.

8.1 Uniqueness

State-of-the-art mesh sizing algorithms, firstly, are known to handle triangular meshes effectively. Not much is known about mesh size control of quadrilateral meshes. Secondly, the size variation in the mesh with existing algorithms is governed by a generic field-type or single function solution. This paper proposes a completely new approach of using a controlled advancing-front technique with both triangles and quadrilaterals to handle local size within a radius of influence. Outside the radius, a more generic field type approach is used. Furthermore, the local size control provided is point-based and thus offers size variation with more accuracy than existing algorithms.

8.2 Flexibility

The proposed mesh size control algorithm is designed to be flexible. It can handle mesh size control at vertices of edges and the interior of edges and faces. Being point and radius based, this size control algorithm is more pin-pointed than other algorithms both in terms of location and radius of influence. When zones of local sizing overlap, the algorithm resolves conflict is an elegant manner by giving proper weightage to the zones in proportion to the geodesic distance between them and their radii of influence. Additionally, since the mesh generated within the radius of control uses a specific algorithm – advancing front, irrespective of the global algorithm of mesh generation used, the local mesh conforms to a particular pattern. This is vastly unlike existing algorithms where mesh size or grading is expressed as a field function and the global meshing algorithm follows it. For different global meshing algorithms the type of mesh generated within the radius of influence, in such cases, will look and feel different. With the algorithm we propose, the mesh within the radius of influence will always look the same irrespective of the global meshing algorithm.

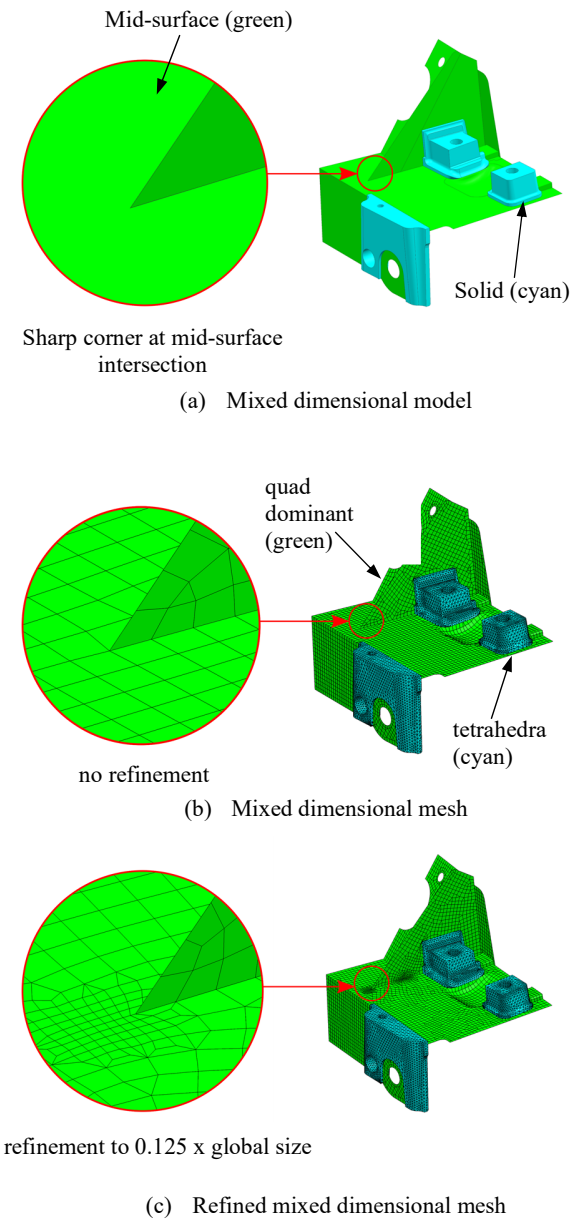

Figure 21. Mesh refinement around sharp features in mixed-dimensional meshing

8.3 User Control

A great deal of user control is provided in a pin-pointed manner. Such accurate user-control also makes it stand apart from existing methods. First of all, the user gets to control local mesh sizing on a surface in three specific ways – a) at a vertex on its boundary b) in the interior of a boundary edge and c) in the interior of the face at specific locations. Figure 21 describes a typical example of how the aforementioned functionality is used in industry today. In mixed dimensional meshing where vast portions of thin-sheet volumes are represented by mid-surfaces, very often at T-junctions, where the mid-sheets intersect sharp corners may occur. To improve the accuracy of the solution in this region it is often desirable to increase the density of the mesh, as shown in figure 21c. Secondly, the spread of the local size is controlled by a radius of influence. Thirdly, the local mesh produced is layered irrespective of the finite element type. This provides, as the fourth control option, a tool to the user to vary thickness of the layer in the first chamber according to certain standard functions like constant, ramp, sinusoidal or parabolic.

9. CONCLUSION

This paper introduces a new type of anisotropy called "Bicameral Anisotropy". Particularly prevalent in automotive, aerospace and electronic industries, bicameral anisotropy is about different size fields in local chambers versus the residual-global chamber that jointly make up the entire geometry meshed. The paper discusses, for a two-dimensional problem, a new approach to controlling local variable sizing.

The first chamber is controlled by constant to linear local size functions. The second chamber, which is called the Residual-Global chamber making up the rest of the geometry, is governed by a nonlinear sizing function leading to transitioning meshes. We propose a controlled advancing front method, in both triangular and quadrangular meshes, that guarantees very high quality, well-controlled local quality metric in the first chamber. An H-shock sizing scheme governs the second chamber. Virtual mesh topology, and loop-segments are constructed at the face boundary both at geometry and nodeloop levels to facilitate this type of bicameral meshing. A wide range of user-control is provided which can allow for flexibility in varying the size-functions on both boundary and in the face-interior of the local chambers. Results clearly indicate the efficacy of the proposed approach leading to both a well controlled desired size field and high local quality in a completely automatic mode.

REFERENCES

[1] M. J. Castro-Diaz, F. Hecht and B. Mohammadi, 'New progress in anisotropic grid adaptation for inviscid and viscid flows simulation', *4th Int. Mesh Roundtable*, Albuquerque, New Mexico (1995).

[2] H. Borouchaki, P. L. George and B. Mohammadi,'Delaunay mesh generation governed by metric specifications. Part II: applications', *Finite Elements Anal. Des*., Vol.25, pp. 85 -109 (1997).

[3] M. Fortin, M. G. Vallet, J. Dompierre, Y. Bourgault and W. G. Habashi, 'Anisotropic mesh adaption: theory, validation and applications', *Eccomas' 96, Paris, CFD Book*, pp.174-199 ,(1996).

[4] R. Verfurth, *A Review of a Posteriori Error Estimation and Adaptive Refinement Techniques*, Wiley, Teubner (1996).

[5] J. Peraire, M. Vahdati, K. Morgan and O. C.Zienkiewicz, 'Adaptive remeshing for compressible flow computations', *J. Comput. Phys*., Vol.72, pp.449 - 466 (1987).

[6] H. Borouchaki, F. Hecht, P.Frey, 'Mesh gradation control', *Int. J. Numer. Meth. Engng*. Vol.43, pp.1143-1165 (1998).

[7] A. Loseille, A Deriveux, F. Alauzet. 'Fully anisotropic goal-oriented mesh adaption for 3D steady state Euler equations. *J. Comput. Phys*., Vol 229. pp. 2866-2897 (2010).

[8] Leicht, T, Hartmann, R. Error estimation and anisotropic mesh refinement for 3d laminar aerodynamic flow simulations. , *J. Comput. Phys*. Vol 229. pp. 7344-7360 (2010).

[9] T. Blacker and M. Stephenson, 'Paving: A new approach to automated quadrilateral mesh generation', *Int. J. Numer. Meth. Engng*., Vol. 32, pp.811-847 (1991).

[10] R. Lohner, 'Progress in grid generation via the advancing front technique', *Engng. With Computers*, Vol.12, pp.186-210 (1996).

[11] N. Mukherjee, 'A Combined Subdivision and Advancing Loop-Front Surface Mesher (Triangular) for Automotive Structures', *Int. J. Vehicle Struct. & Systems*, 2(1), pp.28-37 (2010).

[12] N. Mukherjee, 'CSALF-Q: A Bricolage Algorithm for Anisotropic Quad Mesh Generation', *Proc. XXth International Meshing Roundtable*, Paris, France, pp. 489-510, Springer (2011).

[13] K. Beatty, N. Mukherjee, 'A Transfinite Meshing Approach for Body-In-White Analyses'. *Proc. 19th International Meshing Roundtable*, Springer, pp.49-65 (2010).

[14] N. Mukherjee, 'System, method, and computer program product for smoothing', patent, US 9082220 B2, (July 14, 2015).